Eco-Efficient Hydrolysis of Coconut Oil: Continuous Hydrothermal and Water-Only Process for Sustainable Production of Oleochemicals

Enkeledo Menalla[1], Diego Martin[1], Luis Vaquerizo[1], Jefferson W. Tester[2], María José Cocero[1], Danilo Cantero[1]*

[1] *The Institute of Bioeconomy, Department of Chemical Engineering and Environmental Technology, University of Valladolid, Valladolid, 47011, Spain.*

[2] *Department of Chemical and Biomolecular Engineering, Cornell University, Ithaca, NY, 14853, USA.*

**Corresponding author: Danilo.Cantero@uva.es*

Supplement Information

For clarity, the ESI follow the same section order as the manuscript, enabling direct one to one cross-referencing between sections.

2.1. Materials

For GC–MS analysis, the solvents used were N,O-bis(trimethylsilyl)trifluoroacetamide (BSTFA, Lot 102448727), pyridine (Lot 102471057), and hexadecane (Lot SHBP3147), all obtained from Sigma Aldrich, along with toluene (99.9%) from Applichem Panreac.

Tetrahydrofuran (THF, 99.8%, Lot 2489607) was used both for sample preparation and as the mobile phase in SEC–HPLC analyses. Analytical standards for GC–MS and SEC–HPLC included lauric acid (>98%, Lot MKBS2171V), myristic acid (>98%, Lot BCCC3322), palmitic acid (>98%, Lot BCBX2136), and glycerol (99.5%, Lot BCDS4911V), all purchased from Sigma Aldrich.

Cetearyl alcohol (Lot 10179523) and xanthan gum (Lot 11138-66-2), purchased from Sigma Aldrich, were used as stabilizer and thickener, respectively.

2.5.1. HPSEC (high-performance size-exclusion chromatography)

This technique was applied to analyze triglycerides, diglycerides, monoglycerides, and total fatty acids derived from coconut oil. The analysis utilized three styrene–divinylbenzene copolymer gel columns with pore sizes of 50, 100, and 100 Å, a mobile phase flow rate of 0.8 mL/min, and consistent column and detector temperatures of 35 °C. An injection volume of 20 µL was used. For sample preparation, 100 mg of sample was dissolved in 10 mL of tetrahydrofuran (THF), homogenized for 15 minutes, and filtered through a 0.22 µm nylon filter. Glycerol content was quantified through stoichiometric calculations and gas chromatography. Calibration standards included tristearin, distearin, monostearin, and stearic acid, which served as references for determining the total concentrations of triglycerides, diglycerides, monoglycerides, and fatty acids [1].

2.5.2. Gas chromatography

A gas chromatograph with an HP-5ms capillary column (30 m x 0.25 mm, Agilent Technologies, USA) was used for quantification of free fatty acids (FFA) and glycerol. Calibration lines were prepared using standard free fatty acids from Sigma-Aldrich, including lauric, myristic, and palmitic acids. A glycerol standard was also used for quantification. Approximately 5 mg of each sample was dissolved

in 2 mL of chloroform:methanol (3:1, v/v), sonicated for 20 minutes, and then filtered through 0.22 µm nylon syringe filters. The solvent was evaporated, and samples were derivatized with 250 µL of bis(trimethylsilyl)-trifluoroacetamide (BSTFA) and 50 µL pyridine at 70 °C for 2 hours. Hexadecane in toluene (10 µL/25 mL) served as an internal standard to minimize sample preparation errors [2]. Calibration curves were constructed using various concentrations of each fatty acid standard, following the same preparation steps.

Data were acquired using a quadrupole mass spectrometer (5977A, Agilent Technologies, USA) in splitless mode (1/50) with helium as the carrier gas at 1 mL/min. The oven temperature was programmed as follows: 80 °C (initial), ramped at 2 °C/min to 116 °C, then at 5 °C/min to 176 °C, at 2 °C/min to 270 °C, and finally at 20 °C/min to 310 °C, held for 5 minutes to prevent pyridine detection. Injection volume was 1 µL at 250 °C [3].

2.5.3. Fourier-transform infrared spectroscopy (FT-IR)

This technique was employed to evaluate structural changes in triglycerides before and after hydrolysis using a Bruker Tensor 27 spectrometer. The recorded spectra were baseline-corrected and normalized to the maximum peak intensity, with each spectrum representing the average of 64 individual scans. The samples were analyzed directly without additional preparation.

2.5.4 Total antioxidants

A sample of about 1 g was diluted in 10 mL of methanol. For TPC analysis, 3 mL of Type I water was added to labeled tubes. A 40 µL aliquot of either buffer (blank), standard (gallic acid), or sample was then added and mixed by vortexing. 200 µL of Folin-Ciocalteu reagent was added, and the mixture was allowed to react for 5 minutes, producing a yellow color. Subsequently, 600 µL of 20% Na_2CO_3 was added, and the tubes were incubated at 40°C for 30 minutes. After cooling, absorbance was measured at 765 nm using a spectrophotometer. Calibration was performed with gallic acid standard solutions at varying concentrations [4,5].

2.6.1 Emulsion production

Emulsions were prepared using varying volumes of the product (0.2, 0.4, 0.6, 0.8, 1, 1.2, 1.4, 1.6, 1.8, and 2 mL) combined with 2 mL of water to identify the optimal ratio for stability. The addition of stabilizing agents, including Cetearyl alcohol as a stabilizer and xanthan gum as a thickener, was also evaluated. The emulsions were prepared using an Ultraturrax IKA T25 high-shear homogenizer,

employing two rotational speeds—10,000 rpm and 20,000 rpm—to investigate the effect of shear rate on emulsion formation and stability [6,7]. For each formulation, 2 mL of water was mixed with 1 mL of the product and homogenized for 5 minutes to achieve consistent mixing and effective droplet size reduction. The influence of product concentration, shear rate, and additives on the stability and properties of the emulsions was systematically studied [6,8].

2.6.2 Emulsion analytical: FlowCam

The FlowCam 8000 was employed to analyze the droplet size distribution and morphology of emulsions[9,10]. Two sample dilutions were prepared for analysis: 0.5 g of emulsion was diluted in 99.5 g of distilled water to evaluate emulsion stability, while 0.5 g of emulsion was diluted in 595 g of distilled water to fully disrupt the emulsion and measure individual particle size and distribution. The instrument was calibrated prior to analysis to ensure precise detection of particle sizes and shapes. Imaging was conducted using a 4x objective lens, with measurements performed at a flow rate of 0.8 mL/min to minimize clogging or droplet overlap. Visual and statistical analyses were conducted using FlowCam software to assess droplet stability, size, and distribution.

2.7. Principal Component Analysis (PCA)

Principal Component Analysis (PCA) was employed to reduce the dimensionality of the compositional dataset while preserving the variance essential for understanding sample differences [11]. The analysis focused on the relative concentrations of triglycerides (TG), diglycerides (DG), monoglycerides (MG), free fatty acids (FFA), and glycerol (G).

2.7.1. Data Preprocessing

Prior to PCA, the dataset was normalized to ensure equal weighting of variables, as these features have different units and scales [11]. The standardization followed z-score normalization, calculated as:

$$\chi^{l} = \frac{\chi - \mu}{\sigma} \quad (1)$$

where $x^{'}$ is the standardized value, x is the original value, μ is the mean, and σ is the standard deviation of the variable. This normalization ensures that all variables contribute equally to the analysis.

The covariance matrix of the standardized dataset was computed to capture the linear relationships between variables. The covariance matrix is defined as:

$$Cov(X) = \frac{1}{n-1} X^T X \quad (2)$$

where X is the standardized data matrix ('m x n' with m samples and n features), X^T is its transpose, and n is the number of features.

The principal components were determined by eigenvalue decomposition of the covariance matrix:

$$Con(X) \cdot \mathrm{W} = \lambda \cdot \mathrm{W} \quad (3)$$

where W is the matrix of eigenvectors (principal components), and λ is the diagonal matrix of eigenvalues. The eigenvalues represent the variance explained by each principal component, while the eigenvectors define the directions of maximum variance.

The dataset was then transformed into the principal component space using the relationship:

$$Z = X \cdot \mathrm{W} \quad (4)$$

where Z is the transformed data in the new coordinate system, X is the standardized dataset, and W is the eigenvector matrix.

To assess the contribution of each principal component to the total variance, the explained variance ratio was calculated:

$$E_{VR} = \frac{\lambda_i}{\sum_{j=1}^{n} \lambda_j} \quad (5)$$

Where λ_i is the eigenvalue associated with the i principal component, and n is the total number of components. The first two principal components, accounting for the majority of the variance, were selected for visualization[11].

2.7.2 Clustering Analysis

To identify groups with similar compositional profiles, k-means clustering was applied to the PCA-transformed data. The k-means algorithm partitions the data into k clusters by minimizing the within-cluster sum of squared distances (WCSS):

$$WCSS = \sum_{i=1}^{k} \sum ||\chi - \mu_1||^2 \quad (6)$$

where k is the number of clusters, C_i is the set of points in the i cluster, x represents a data point, and μ_i is the centroid of the cluster. The clustering results provided insights into sample groupings based on their compositional profiles [12].

2.8. Kinetic Model of Triglycerides (Severity factor t_s)

The kinetic parameters were determined relying on the studies conducted by Minami – Saka[13], Milliren [14], and Savage[15] who also investigated the influence of fatty acids acting as autocatalysts. These reactions are shown in equation 7 to 12.

$$TG + H_2O \Leftrightarrow DG + FFA \quad (7)$$

$$DG + H_2O \Leftrightarrow MG + FFA \quad (8)$$

$$MG + H_2O \Leftrightarrow G + FFA \quad (9)$$

$$TG + H_2O + FFA \Leftrightarrow DG + 2FFA \quad (10)$$

$$DG + H_2O + FFA \Leftrightarrow MG + 2FFA \quad (11)$$

$$MG + H_2O + FFA \Leftrightarrow G + 2FFA \quad (12)$$

A simplified reaction rate approach is used to construct a kinetic model for the hydrolysis reactions. The rate of each reaction is proportional to the concentration of the reactants. The rate constants for each step are denoted as k0, k1, and k2 for the first, second, and third reactions, respectively. The rate equations can be written as shown in equations 7 to 12.

$$\frac{dC_{TG}}{dt} = \left(-k_0 C_{TG} C_{H_2O} + k_{0_{-1}} C_{DG} C_{FFA}\right) x C_{FFA} \quad (13)$$

$$\frac{dC_{DG}}{dt} = \left(k_0 C_{TG} C_{H_2O} - k_{0_{-1}} C_{DG} C_{FFA} - k_1 C_{DG} C_{H_2O} + k_{1_{-1}} C_{MG} C_{FFA}\right) x C_{FFA} \quad (14)$$

$$\frac{dC_{MG}}{dt} = \left(k_1 C_{DG} C_{H_2O} - k_{1_{-1}} C_{MG} C_{FFA} - k_2 C_{MG} C_{FFA} + k_{2_{-1}} C_G C_{FFA}\right) x C_{FFA} \quad (15)$$

$$\frac{dC_G}{dt} = \left(k_{2_{-1}} C_G C_{FFA} + k_2 C_{MG} C_{FFA}\right) x C_{FFA} \quad (16)$$

$$\frac{dC_{FFA}}{dt} = \begin{pmatrix} -k_{0_{-1}} C_{DG} C_{FFA} + k_0 C_{TG} C_{FFA} - k_{1_{-1}} C_{MG} C_{FFA} + k_1 C_{DG} C_{FFA} \\ -k_{2_{-1}} C_G C_{FFA} + k_2 C_{MG} C_{H_2O} \end{pmatrix} x C_{FFA} \quad (17)$$

$$\frac{dC_{H_2O}}{dt} = \begin{pmatrix} -k_0 C_{TG} C_{H_2O} + k_{0_{-1}} C_{DG} C_{FFA} - k_1 C_{DG} C_{H_2O} + k_{1_{-1}} C_{MG} C_{FFA} \\ -k_2 C_{MG} C_{H_2O} + k_{2_{-1}} C_G C_{FFA} \end{pmatrix} x C_{FFA} \quad (18)$$

The ODE system for the kinetic model is simple and was solved using forward Euler's method implemented in cells of a Microsoft Excel datasheet. A fixed time step of 0.01 min was sufficient to solve the system with enough precision. The objective function (OF) was computed as the sum of the squares of the percentage error between the amounts of the components that were measured experimentally and determined numerically by simulation. The objective function was minimized

using the Solver add-in fitting the ki (k_0, $k_{0_{-1}}$, k_1, $k_{1_{-1}}$, k_2, $k_{2_{-1}}$)of the different equations. Finally, the Arrhenius equation was used to determine the activation energy.

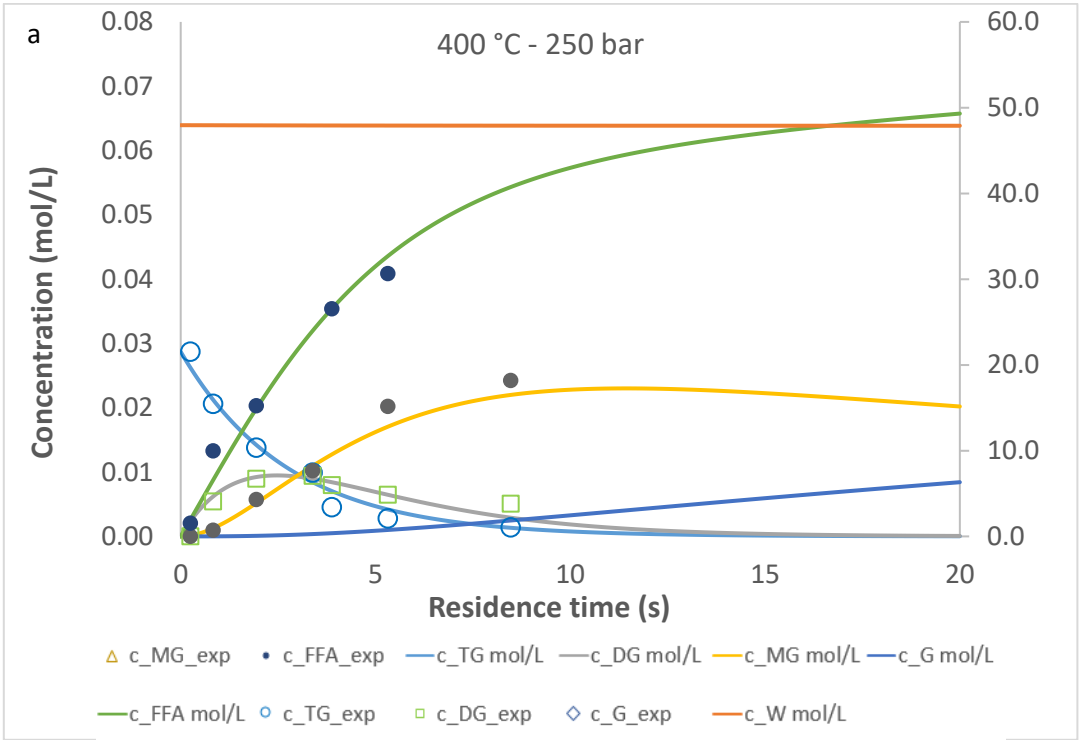

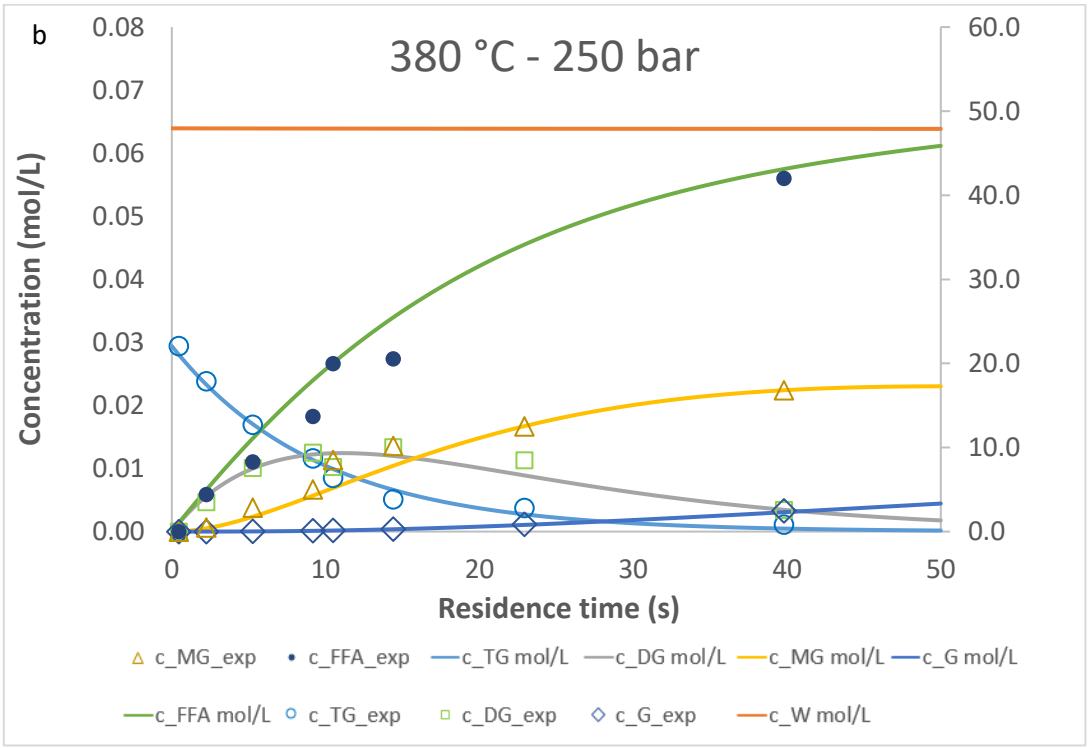

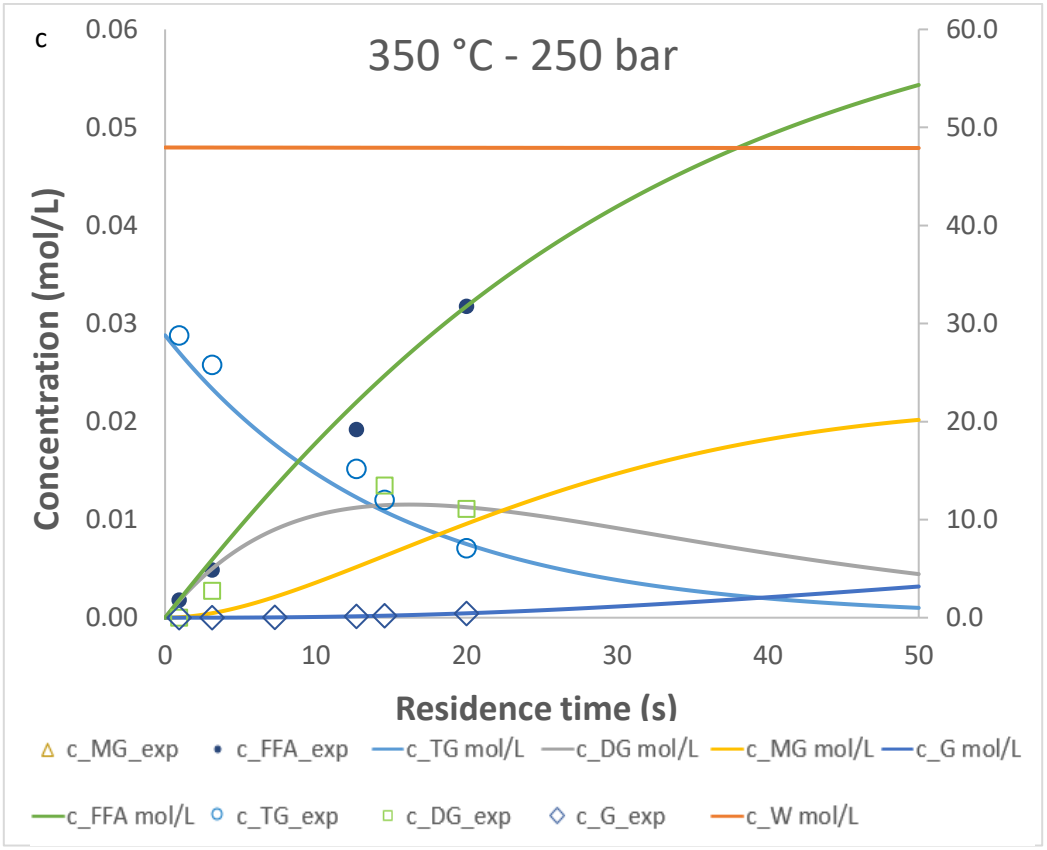

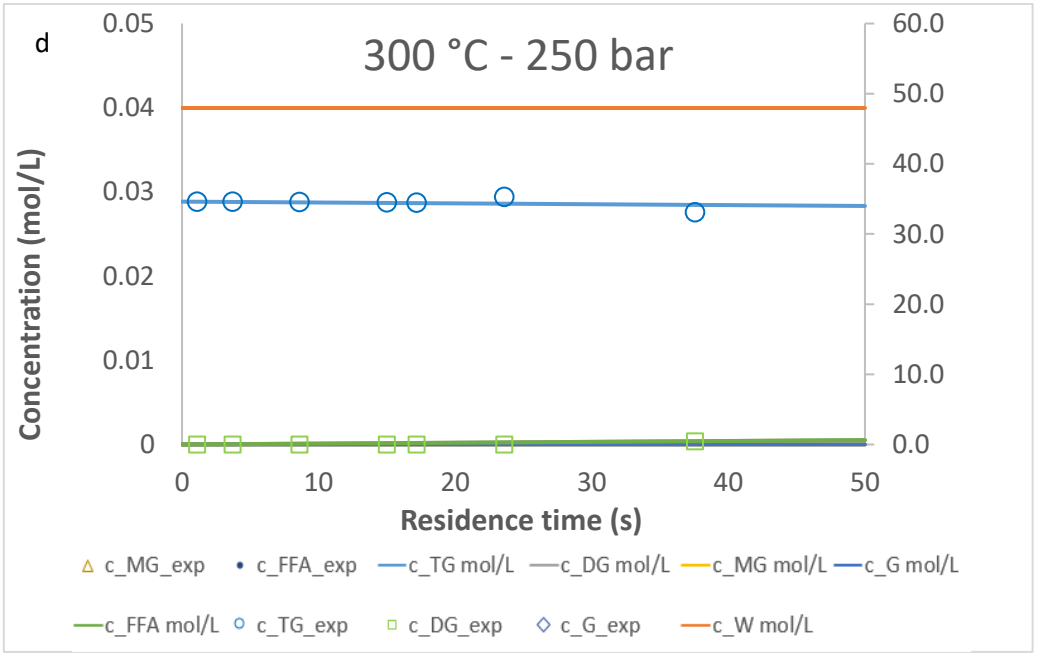

Fig. S1. Kinetic model fit for conditions: a: 400 ◦C – 25.0 MPa, b: 380 ◦C – 25.0 MPa, c: 350 ◦C – 25.0 MPa and d: 300 ◦C – 22.0 MPa, over time

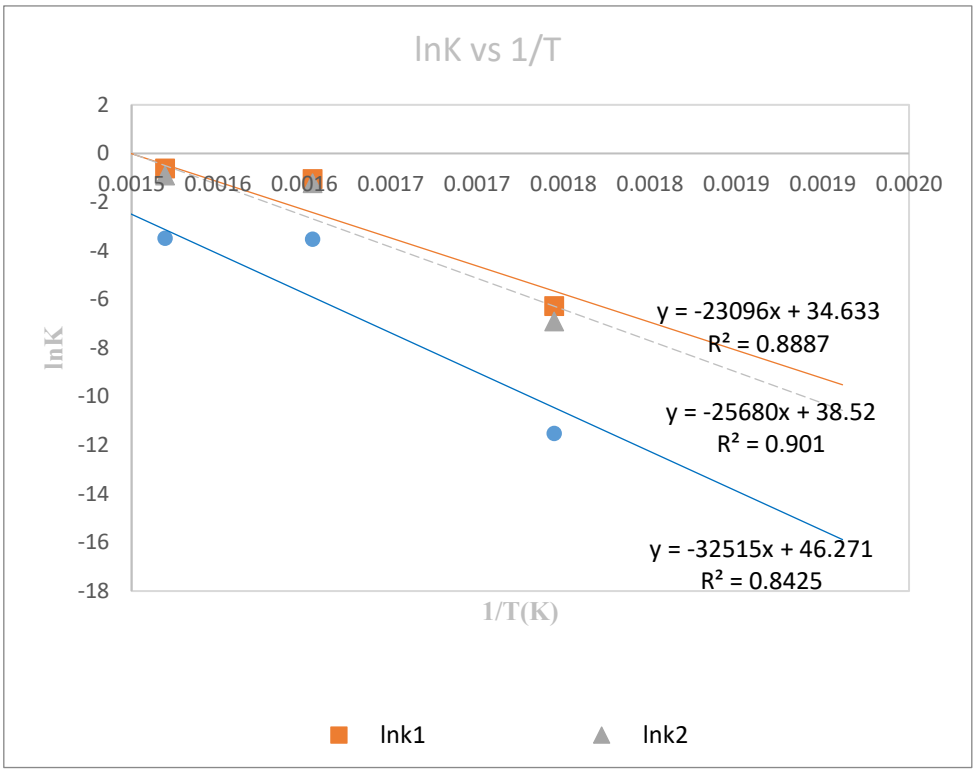

Fig. S2. Arrhenius plot for triglyceride hydrolysis.

Table S1. Kinetic parameters for triglyceride hydrolysis

Temperature (ºC)	Pressure (MPa)	k_1	k_2	k_3
250	220	0	0	0
300	220	0.00	0.00	0.00
350	250	0.35	0.29	0.03
380	250	0.54	0.40	0.03
400	250	0.75	0.93	0.05
E_{a1}		192.02	-	-
E_{a2}		-	213.50	-
E_{a3}		-	-	270.33
lnA		34.63	38.52	46.27

2.8.1 Severity Factor Calculations

The calculation of the Severity Factor is based on real data from the kinetic model and the activation energy.

a

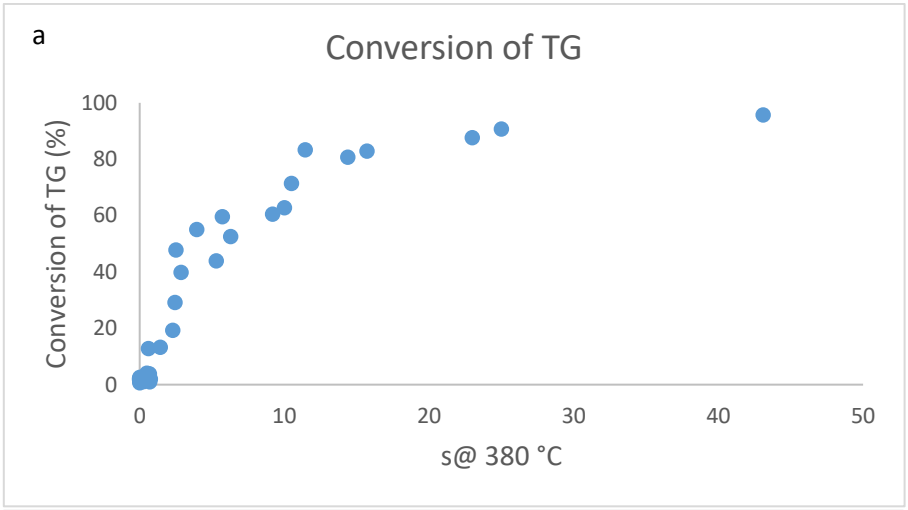
Conversion of TG
Conversion of TG (%)
100
80
60
40
20
0
0
10
20
30
40
50
s@ 380 °C

b

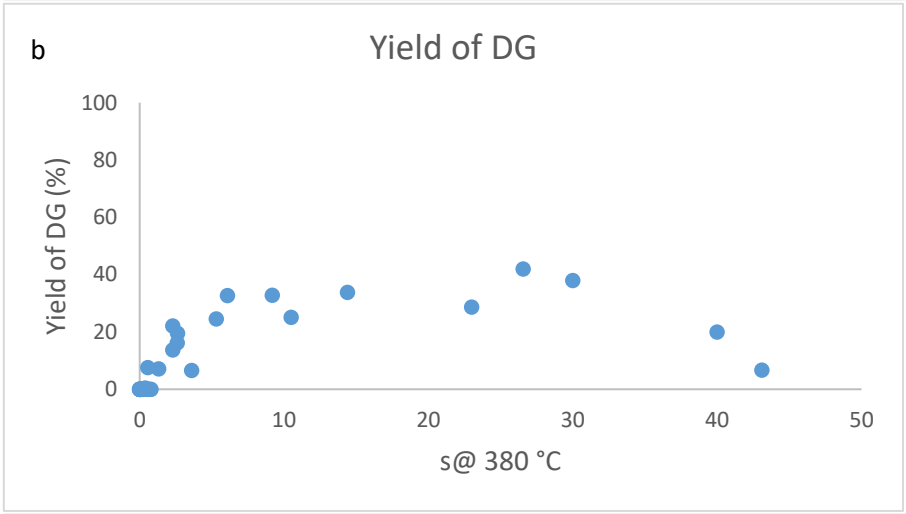
Yield of DG
Yield of DG (%)
100
80
60
40
20
0
0
10
20
30
40
50
s@ 380 °C

c

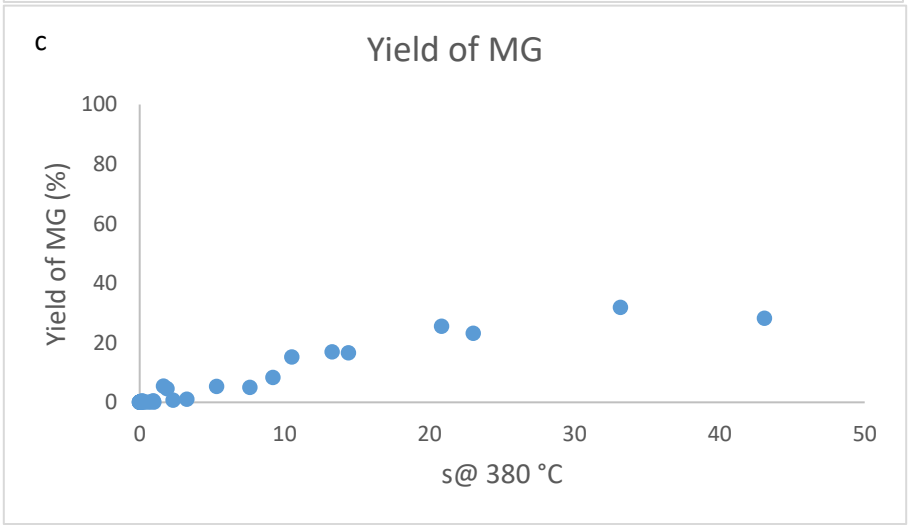
Yield of MG
Yield of MG (%)
100
80
60
40
20
0
0
10
20
30
40
50
s@ 380 °C

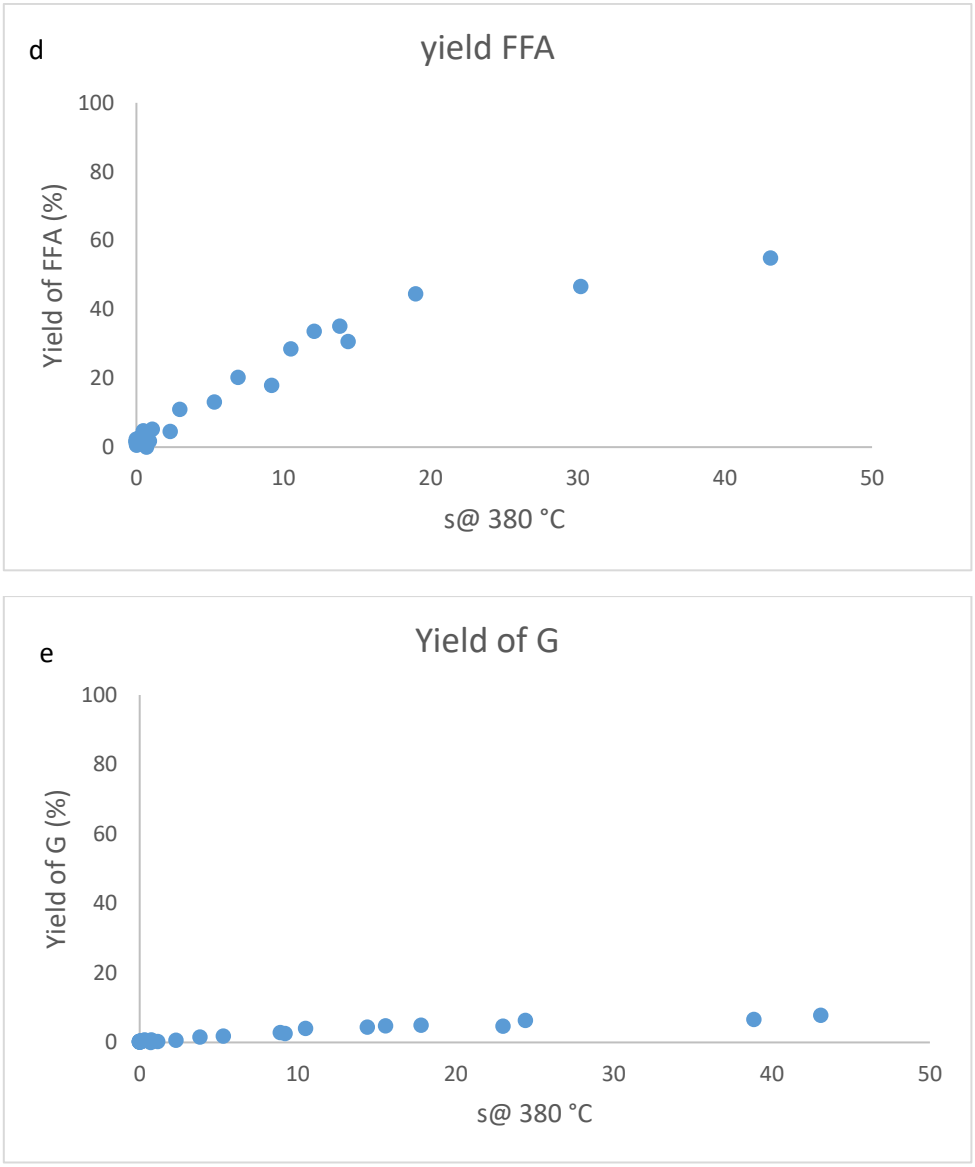

Fig. S4. Coconut oil hydrolysis profile at 380 °C as a function of severity time, showing the conversion/Yield of (a) triglycerides (TG), (b) diglycerides (DG), (c) monoglycerides (MG), (d) free fatty acids (FFA), and (e) glycerol (G) over time.

3.1 Hydrolysis of Coconut Oil.

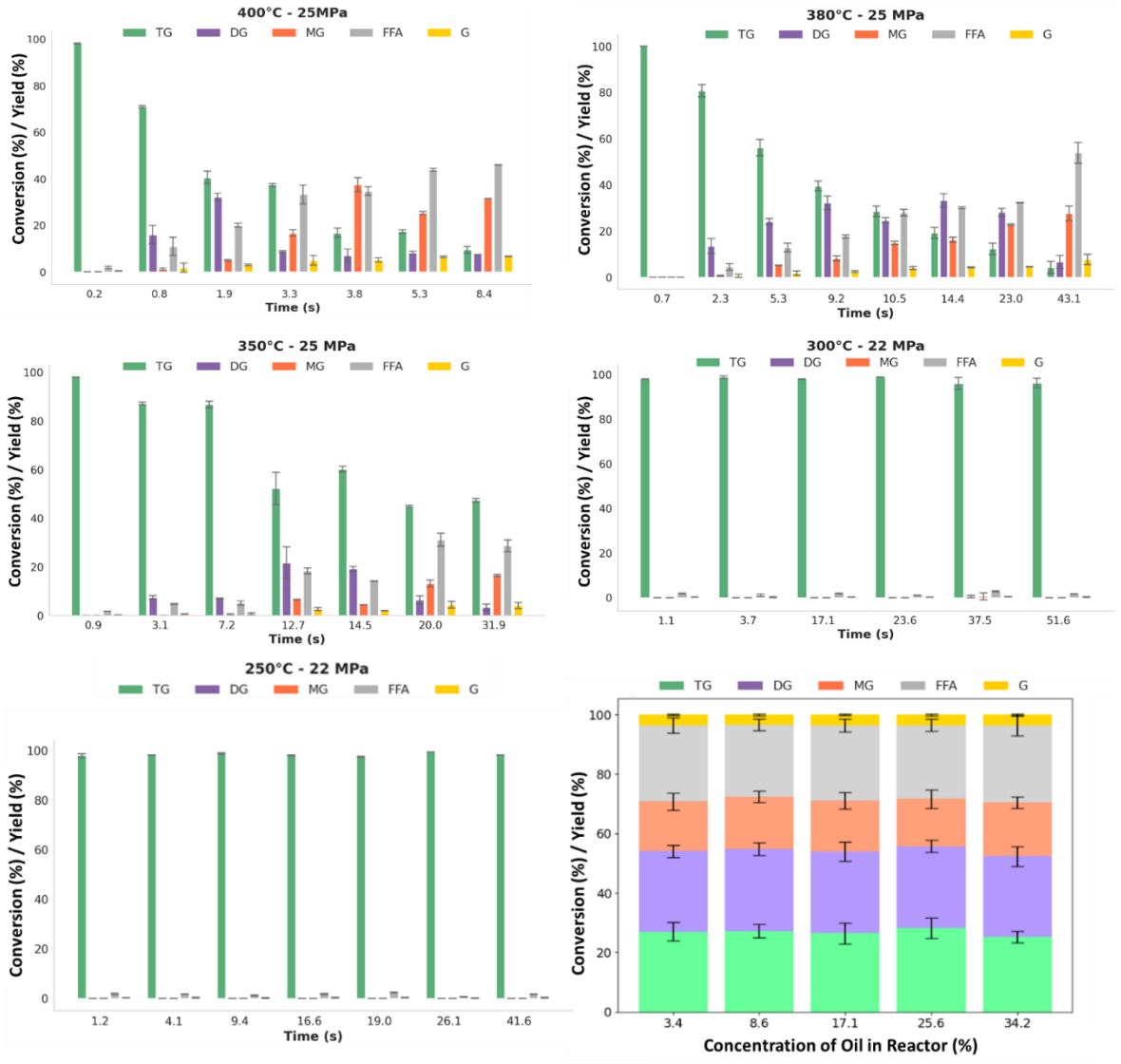

Fig. S5. Coconut oil hydrolysis and product conversion at a: 400 ◦C – 25.0 MPa, b: 380 ◦C – 25.0 MPa, c: 350 ◦C – 25.0 MPa, d: 300 ◦C – 22.0 MPa, e: 250 ◦C – 22.0 MPa over time, f: 380 ◦C – 25.0 MPa with different inlet concentration of raw material (Oil) in the reactor.

4.1 Green Chemistry Metrics

Green chemistry metrics were calculated based on the concentration profiles of triglycerides (TG), diglycerides (DG), monoglycerides (MG), glycerol (G), and free fatty acids (FFA) obtained from

continuous hydrolysis of coconut oil in subcritical water. All concentrations were expressed in mass units.

The following standard green chemistry metrics were computed:

Atom Economy (AE):

$$AE = \frac{(Molecular\ weight\ of\ DG, MG, FFA, G)^p}{(Molecular\ weight\ of\ (TG)^R}$$

Process Mass Intensity (PMI):

$$PMI = \frac{(Mass\ of\ TG)^R}{(Mass\ of\ TG, DG, MG, FFA, G)^p}$$

Reaction Mass Efficiency (RME):

$$RME = \frac{(Mass\ of\ TG, DG, MG, FFA, G)^p}{(Mass\ of\ TG)^R}$$

E-factor:

$$E - factor = \frac{(Mass\ of\ TG)^p}{(Mass\ of\ DG, MG, FFA, G)^p}$$

Energy Intensity (EI):

$$EI(\frac{MJ}{kg}) = \frac{(Total\ Energy\ Input)}{(Mass\ of\ DG, MG, FFA, G)}$$

Table S2. Representative mass balances and operating conditions for basic, acidic, and enzymatic triglyceride hydrolysis (normalized to 100 g TG feed)

Basic Hydrolysis		**Acidic Hydrolysis**		**Enzymatic Hydrolysis**	
Parameter/Component	Value/Details	Component	Mass (g)	Component	Mass (g)
T / Time	70–80°C / 1-3h	T / Time	110–150°C / 4–8 h	T / Time	35–45°C / 4–6 h
Oil (TG input)	100.0 g	Oil (TG input)	100	Oil (TG input)	100
NaOH (input)	92.6 g	Catalyst (solid/H_2SO_4)	5	Lipase (CRL/Lipozyme)	2
Water (input)	370.4 g	Water (rxn input)	200	Phosphate buffer pH 7.5	250
Ethanol (input)	351.9 g	Subtotal Rxn	305	Total Input	352

HCl (pure equiv., acidif.)	60.0 g	Hexane (extraction)	200	FFA (dried product)	89.8
HCl water (37%)	102.0 g	Grand Total Input	505	Glycerol (aq waste)	10.2
NaCl (brine)	150.0 g	FFA (product, dried)	92	Lipase recovered	1.8
Total Input	1226.8 g	Glycerol (aq waste)	8	Recovered buffer	175
FFA (dried product)	90.9 g	Catalyst recovered	4.8	Wash loss (rinses)	25
Glycerol (aq)	9.1 g	Recovered water	120	Evaporated/residue	15
Salts (NaCl/excess)	211.0 g	Recovered hexane	180	Total Output	320.8
Recovered solvents	618.2 g	Evaporated water/hexane	35		
Evaporated solvents	108.3 g	Wash/seps waste	80		
Wash water loss	80.0 g	Total Output	521.8		
Filtration loss	8.0 g				
Total Output	1126 g				
References	[16–21]	References	[16,22–26]	References	[27–31]

The data in Table S2 summaries representative mass balances (normalized to 100 g triglyceride feed) for basic, acidic, and enzymatic hydrolysis, including reaction conditions, major inputs (reagents, water/solvents, catalysts/enzymes), and key outputs (dried free fatty acids, glycerol-containing aqueous streams, salts, and recoverable auxiliaries). This side-by-side format highlights the main process burdens that differentiate the routes—namely neutralization salt formation and higher auxiliary usage in basic hydrolysis, solvent-assisted separation requirements in acidic hydrolysis, and the reliance on buffer and enzyme handling in enzymatic hydrolysis—providing the basis for subsequent calculation and comparison of green metrics (PMI, E-factor, and RME).

Table S3. Environmental Impact Metrics Over Time without Water Recovery

Time (s)	Products (g)	PMI (No Water Recovery)	E-factor (No Water Recovery)	RME (No Water Recovery)
2.3	19.30±0.77	14.80±0.44	13.80±0.41	0.06±0.002
9.2	60.49±2.12	4.72±0.14	3.72±0.11	0.21±0.006
14.4	83.78±2.51	3.41±0.10	2.41±0.07	0.29±0.009
23	87.72±1.75	3.26±0.10	2.26±0.07	0.30±0.009
43.1	95.78±1.15	2.98±0.09	1.98±0.06	0.33±0.010

The table S3 summarizes the evolution of Green Chemistry metrics for supercritical water hydrolysis as a function of residence time, using a basis of 100 g of organic material and a reactor composition of 35 wt% oil and 65 wt% water without water recovery. As residence time increases from 2.3 to 43.1 s, the mass of hydrolysis products (DG + MG + FFA + glycerol) increases steadily, reflecting enhanced triglyceride conversion. This improvement in conversion is directly translated into progressively better process metrics, with the process mass intensity (PMI) decreasing from 14.80 to 2.98, the E-factor decreasing from 13.80 to 1.98, and the reaction mass efficiency (RME) increasing from 0.06 to 0.33. Although the values reported correspond to a scenario without water recovery, in table 5 of the article the data represent water recovery is considered. Experimental operation indicates that 50–90% of the process water can be recovered; for comparative calculations, a conservative and realistic intermediate value of 70% water recovery was used in calculations.

References

1 ISO 113581, *Int. Organ. Stand.*, 2015, **10406**–**1:20**, 3–6.

2 F. Rezaei, R. Jamei and R. Heidari, *Adv. Pharm. Bull.*, 2018, **8**, 115–121.

3 J. D. McCurry, *Technology*, 2008, 1–10.

4 R. Kumar and P. Singh, *J. Herb. Med.*, 2025, **49**, 100982.

5 I. G. Hwang, Y. J. Shin, S. Lee, J. Lee and S. M. Yoo, *Prev. Nutr. Food Sci.*, 2012, **17**, 286–292.

6 Y. J. Kim, I. Y. Lee, T. Kim, J. H. Lee, Y. G. Chun, B. Kim and M. H. Lee, *J. Sci. Food Agric.*, 2022, **102**, 5738–5749.

7 Y. Bao, H. Xue, Y. Yang, X. Wang, H. Yu and C. Piao, *Foods*, 2021, **10**, 2982.

8 A. Acero-Lopez, P. Schell, M. Corredig and M. Alexander, *J. Dairy Res.*, 2010, **77**, 445–451.

9 G. T. Karsli, S. Şahin and M. H. Öztop, *Acs Food Sci. Technol.*, 2022, **2**, 1832–1839.

10 Q. Fu, L. Zhou, H. Shi, R. Wang and L. Yang, *Front. Nutr.*, DOI:10.3389/fnut.2023.1125312.

11 M. Ringnér, *Nat. Biotechnol.*, 2008, **26**, 303–304.

12 P. G. C. Lucena, J. C. Carregosa, M. N. Eberlin, A. Wisniewski and J. M. Santos, *Fuel*, 2025, **384**, 133894.

13 E. Minami and S. Saka, *Fuel*, 2006, **85**, 2479–2483.

14 A. L. Milliren, J. C. Wissinger, V. Gottumukala and C. A. Schall, *Fuel*, 2013, **108**, 277–281.

15 T. Pinnarat and P. E. Savage, *J. Supercrit. Fluids*, 2010, **53**, 53–59.

16 R. A. Sheldon, *Green Chem.*, 2023, **25**, 1704–1728.

17 A. Mannu, P. Almendras Flores, F. Briatico Vangosa, M. E. Di Pietro and A. Mele, *RSC Sustain.*, 2024, **3**, 300–310.

18 E. O. Ebikade, S. Sadula, Y. Gupta and D. G. Vlachos, *Green Chem.*, 2021, **23**, 2806–2833.

19 2019, 3–7.

20 US9745541B1, 2017, 2.

21 Chemistry Education Research and Practice, *R. Soc. Chem.*

22 F. O. Nitbani, P. J. P. Tjitda, B. A. Nurohmah and H. E. Wogo, *J. Oleo Sci.*, 2020, **69**, 277–295.

23 F. Su and Y. Guo, *Green Chem.*, 2014, **16**, 2934–2957.

24 M. A. Peters, C. T. Alves, J. Wang and J. A. Onwudili, *ACS Omega*, 2022, **7**, 46870–46883.

25 K. Ngaosuwan, E. Lotero, K. Suwannakarn, J. G. Goodwin and P. Praserthdam, *Ind. Eng. Chem. Res.*, 2009, **48**, 4757–4767.

26 N. a Serri, a H. Kamarudin and S. N. Abdul Rahaman, *J. Phys. Sci.*, 2008, **19**, 79–88.

27 T. A. V. Nguyen, T. D. Le, H. N. Phan and L. B. Tran, *Scientifica (Cairo).*, 2018, **2018**, 1–6.

28 H. Wang, H. P. Li, C. K. Lee, N. S. Mat Nanyan and G. S. Tay, *Heliyon*, 2024, **10**, e31292.

29 E. Faillace, V. Brunini-Bronzini de Caraffa, M. Mariani, L. Berti, J. Maury and S. Vincenti, *Int. J. Mol. Sci.*, DOI:10.3390/ijms241512274.

30 B. C. Páez, A. R. Medina, F. C. Rubio, P. G. Moreno and E. M. Grima, *Enzyme Microb. Technol.*, 2003, **33**, 845–853.

31 A. Baena, A. Orjuela, S. K. Rakshit and J. H. Clark, *Chem. Eng. Process. - Process Intensif.*, DOI:10.1016/j.cep.2022.108930.